

# Radius of Curvature and Location Estimation of Cylindrical Objects with Sonar using a Multi-sensor Configuration

Ali Safak Sekmen

*Department of Electrical and Computer  
Engineering, Vanderbilt University,  
Nashville, TN 37235 USA  
sekmen@vuse.vanderbilt.edu*

Billur Barshan

*Department of Electrical Engineering  
Bilkent University  
Bilkent, 06533 Ankara TURKEY  
billur@ee.bilkent.edu.tr*

## Abstract

*Although acoustic sensors are inexpensive and convenient to use in time-of-flight (TOF) ranging systems, they have some important limitations one of which is their low angular resolution that makes localization difficult. In this paper, an adaptive multi-sensor sonar system is introduced to compensate for the low angular resolution and improve the localization accuracy. The sensor configuration is used to estimate the radius of curvature and location of cylindrical objects. Sensitivity analysis of the curvature estimate with respect to some measurement errors and certain system parameters is provided. Two methods of TOF estimation are used and compared: thresholding and curve-fitting methods. Theory and simulations are verified by experimental data from a real sonar system. The adaptive configuration improves the estimates by 35-45% and the curve-fitting method, compared to the thresholding, brings an improvement of about 30% in the absence of noise and 50% in the presence of noise. The radius of curvature estimation is shown to be useful for target discrimination.*

## 1. Introduction

One of the major limitations of acoustic sensors is their high beamwidth that reduces the localization accuracy. An adaptive sonar sensor configuration consisting of three transmitter/receiver ultrasonic transducers is used to increase the localization accuracy. With this configuration, the radius of curvature and location of cylindrical objects are estimated. The radius of curvature estimate can be used to differentiate basic types of reflectors. For large values of radius, the target can be assumed to be a planar wall, and for values close to zero, it can be assumed to be an edge.

Sonar sensors have been widely used in robotics applications including underwater robotics. Several researchers used different sensor configurations. Kuc used a system which adaptively changes its position and

configuration in response to the echoes it detects [1]. In [2], Kleeman and Kuc classified target primitives as plane, corner, edge, and unknown. Flynn combined infrared and sonar sensors to compensate for the high beamwidth of sonar sensors [3]. In [4], Sabattini illustrated that advanced filtering techniques are required for making sonar data more accurate and reliable. Peremans *et al* used a linear configuration with three ultrasonic transducers [5].

When the reflection point of the object is not along the line-of-sight (LOS) of the ultrasonic transducer, there is an exponential decline in the amplitude of the reflected sonar signal which decreases the signal-to-noise (SNR). Depending on the orientation of the target, the transducers of the configuration are rotated towards the target to obtain more accurate estimates.

In Section 2, the adaptive sensor configuration is described and the reason to use this configuration is explained. The radius of curvature and location estimation algorithm is presented in Section 3. Two methods of TOF are described in Section 4. Section 5 provides sensitivity analysis of curvature estimation. The simulation results are presented in Section 6. In section 7, the experimental results are illustrated. Finally, some conclusions are drawn in Section 8.

## 2. Multi-sensor Sonar Configuration

For a cylindrical target at range  $z$  and making an angle  $\mathbf{a}$  with the LOS of an ultrasonic transducer, the received time signal reflected by the target is a sinusoidal enveloped by a Gaussian which is given by [6]:

$$S_{z,\mathbf{a}}(t) = \mathbf{r}_c \frac{A_{\max} z_{\min}^{3/2}}{z^{3/2}} e^{-\frac{a^2}{s_a^2}} e^{-\frac{(t-t_0-3/f_0)^2}{2s_t^2}} \sin[2\pi f_0(t-t_0)] \quad (1)$$

where  $z$  is the distance between the transducer and the surface of the object,  $\mathbf{r}_c$  is the reflection coefficient

which increases with the radius of curvature,  $A_{\max}$  is the maximum amplitude,  $z_{\min} \cong a^2 / I$  ( $a$  is the radius of the transducer aperture),  $\mathbf{a}$  is the deviation angle from the LOS,  $\mathbf{s}_a = \mathbf{a}_o / 2$  ( $\mathbf{a}_o$  is the half beamwidth angle),  $t_o$  is the time-of-flight,  $f_o$  is the resonant frequency, and  $\mathbf{s}_t = 1 / f_o$ .

Equation (1) shows that when the deviation angle between the object and sensor is not zero ( $\mathbf{a} \neq 0$ ), there is an exponential decline in the amplitude of the reflected sonar signal. Hence, as the deviation angle increases, SNR decreases. Therefore, sonar data is most reliable when the target lies along the LOS of the transducer, and at nearby ranges due to the  $1/z^{3/2}$  term in Equation (1). In this study, a sensor configuration composed of three ultrasonic transducers is used as shown in Figure 1. First, linear configuration of these sensors are used and some measurement are taken, and then, the transducers are rotated around their center according to these measurements to make them perpendicular to the target.

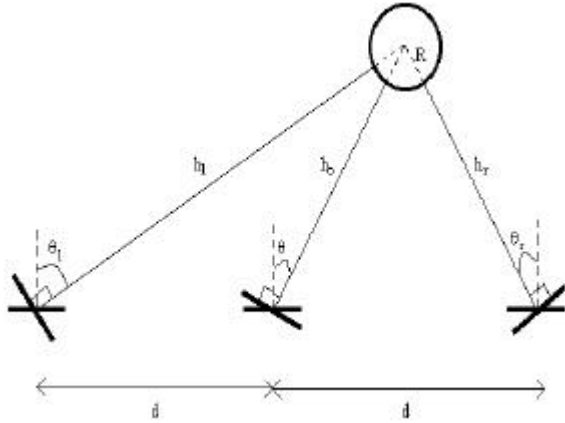


Figure 1. The sensor and target configuration.

### 3. Algorithm

A cylindrical object with radius  $R$  and orientation  $\mathbf{q}$  is considered. The radius of curvature ( $R$ ), the distance between the central transducer and the center of the target ( $r = h_o + R$ ), and the deviation angle of the central transducer ( $\mathbf{q}$ ) are estimated as follows:

- The following measurements are taken by the transducers:

$$\begin{aligned} \hat{h}_o &= \frac{ct_o}{2} = r - R + n_o \\ \hat{h}_r &= \frac{ct_r}{2} = \sqrt{r^2 + d^2 - 2dr \sin \mathbf{q}} - R + n_r \\ \hat{h}_l &= \frac{ct_l}{2} = \sqrt{r^2 + d^2 + 2dr \sin \mathbf{q}} - R + n_l \end{aligned} \quad (2)$$

where  $h_o$ ,  $h_r$ , and  $h_l$  are the distances between the surface of the object and the central, right, left transducers respectively.  $t_o$ ,  $t_r$ , and  $t_l$  are the TOFs for the central, right, and left transducer respectively.  $d$  is the transducer separation.  $n_o$ ,  $n_r$ , and  $n_l$  are noise terms that can be modeled as spatially uncorrelated Gaussian noise since the noise correlation coefficient is small for the acoustic transducers (most of the noise on the sensors is dominated by the thermal noise) [5].

- The probability density function of the measurement vector  $\hat{\mathbf{z}}$  is given as:

$$p_{\hat{\mathbf{z}}} = \frac{1}{2\pi|C|} \exp\left\{-\frac{1}{2}[\hat{\mathbf{z}} - h(r, \mathbf{q}, R)]^T C^{-1}[\hat{\mathbf{z}} - h(r, \mathbf{q}, R)]\right\} \quad (3)$$

where the vectors  $\hat{\mathbf{z}}$ ,  $h(r, \mathbf{q}, R)$ , and the error correlation matrix  $C$  are given by

$$\hat{\mathbf{z}} = \begin{bmatrix} \hat{h}_o \\ \hat{h}_r \\ \hat{h}_l \end{bmatrix}, \quad h(r, \mathbf{q}, R) = \begin{bmatrix} r - R \\ \sqrt{r^2 + d^2 - 2dr \sin \mathbf{q}} - R \\ \sqrt{r^2 + d^2 + 2dr \sin \mathbf{q}} - R \end{bmatrix} \quad (4)$$

$$C = \begin{bmatrix} \mathbf{s}_{n_o}^2 & 0 & 0 \\ 0 & \mathbf{s}_{n_r}^2 & 0 \\ 0 & 0 & \mathbf{s}_{n_l}^2 \end{bmatrix}$$

(5)

- The  $r$ ,  $\mathbf{q}$ , and  $R$  values maximizing Equation (3) are the maximum likelihood estimates which can be found by taking the inverse of  $\hat{\mathbf{z}} = h(\hat{r}, \hat{\mathbf{q}}, \hat{R})$  as:

$$\hat{r} = \frac{2d^2 + 2(\hat{h}_l + \hat{h}_r)\hat{h}_o - 2\hat{h}_o^2 - \hat{h}_l^2 - \hat{h}_r^2}{2\hat{h}_r^2 + 2\hat{h}_l^2 - 4\hat{h}_o^2} \quad (6)$$

$$\hat{\mathbf{q}} = \sin^{-1} \left[ \frac{\hat{h}_l^2 - \hat{h}_r^2 + 2(\hat{h}_l - \hat{h}_r)\hat{R}}{4d(\hat{h}_o + \hat{R})} \right] \quad (7)$$

$$\hat{R} = \frac{(\hat{h}_r^2 + \hat{h}_l^2) - 2(\hat{h}_o^2 + d^2)}{4\hat{h}_o - 2(\hat{h}_r + \hat{h}_l)}$$

(8)

- The deviation angles for the right and left transducers are given by

$$\hat{q}_l = \sin^{-1} \left( \frac{(\hat{h}_l + \hat{R})^2 - (\hat{h}_o + \hat{R})^2 + d^2}{2d(\hat{h}_l + \hat{R})} \right) \quad (9)$$

$$\hat{q}_r = \sin^{-1} \left( \frac{(\hat{h}_r + \hat{R})^2 - (\hat{h}_o + \hat{R})^2 + d^2}{2d(\hat{h}_r + \hat{R})} \right) \quad (10)$$

- The left, central, and right transducers are rotated by  $\hat{q}_l$ ,  $\hat{q}_o$ , and  $\hat{q}_r$  respectively and  $r$ ,  $q$ , and  $R$  are estimated again.

#### 4. TOF Estimation

In this study, two methods of TOF estimation are used. The first one, *thresholding*, is the most common method in TOF ranging systems. When a pulse transmitted by the sensor encounters an object, an echo is produced and the TOF of the pulse is considered to be the first time value at which the amplitude of the echo exceeds a preset threshold value. Although the thresholding method is very fast, it is not accurate enough for some applications. The second method of this study, *curve-fitting*, is employed to decrease the error in TOF estimation by thresholding. In this method, a parabolic curve of the form  $a_o(t-t_o)^2$  is fitted to the onset of the sonar echo. First initial estimates of the two parameters  $a_o$  and  $t_o$  are obtained by using samples of the signal around the thresholding point. Initial estimate for  $t_o$  is found by simple thresholding, and  $a_o$  is estimated from the second derivative approximation around the thresholding point [7]. The iterative Lavenberg-Marquart nonlinear least-square algorithm is initialized by these values. To estimate  $a_o$  and  $t_o$ , 50 samples of echo around the threshold point have been used in simulations and experiments. The methods are illustrated in Figure 2.

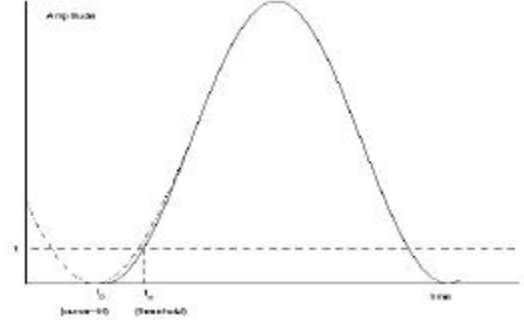
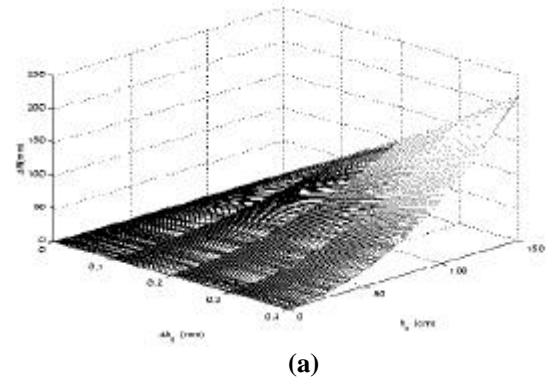


Figure 2. TOF estimate.

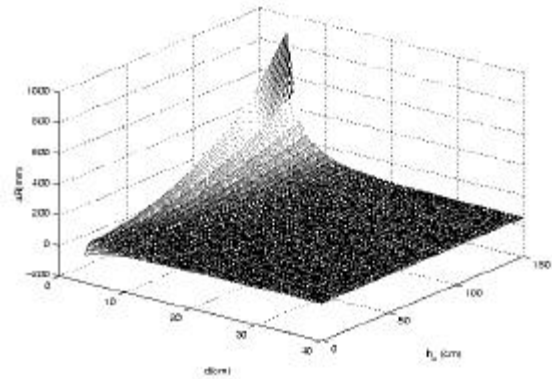
#### 5. Sensitivity Analysis

To illustrate how some measurement errors and certain system parameters affect the radius of curvature estimate, a sensitivity analysis has been provided. A small perturbation is added to a variable and the change in the radius of curvature estimate has been observed. For example, the error,  $\Delta h_l$ , in the left transducer measurement affects the curvature estimate as:

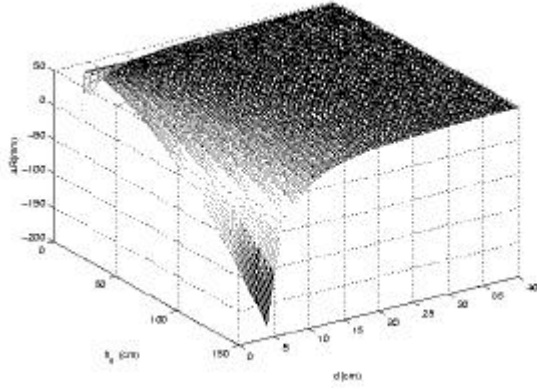
$$\Delta R = \frac{(h_r^2 + (h_l + \Delta h_l)^2) - 2(h_o^2 + d^2)}{4h_o - 2(h_r + h_l + \Delta h_l)} - \frac{(h_r^2 + h_l^2) - 2(h_o^2 + d^2)}{4h_o - 2(h_r + h_l)} \quad (11)$$



(a)



(b)



(c)

**Figure 3.** Sensitivity analysis.

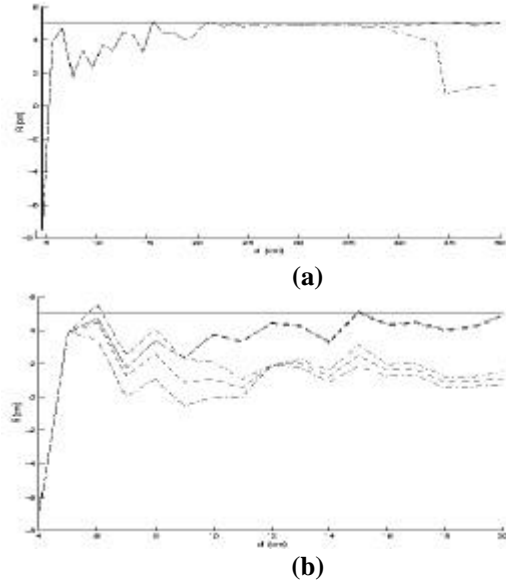
For sensitivity analysis, a stationary cylindrical object at  $q = 0^\circ$  with radius 5 cm is considered. Figure 3(a) illustrates the effect of an error, varying between 0-0.4 mm, in  $h_c$ . The transducer separation is set to 10 cm. The error in  $R$  increases linearly with  $\Delta h_c$  and nonlinearly with  $h_c$  itself. Also, a positive error in  $h_c$  leads a positive error in  $R$  since for constant  $h_r$  and  $h_c$ , increasing  $h_c$  causes an overestimate as shown in Figure 1. Figure 3(b) and (c) display the effect of  $d$  on the  $R$  estimate when the constant errors  $\Delta h_r = 0.18$  mm and  $\Delta h_c = 0.18$  mm are added respectively. For small values of  $d/h_c$ , the error is high since the resolution provided by the differential TOF information between the central and surrounding transducers will not be sufficiently large to estimate the curvature reliably. Hence, as range increases, the transducer separation should also be increased to achieve a higher resolution.

## 6. Simulation Results

The reflected sonar signal is modeled by Equation (1) for the simulations with  $A_{\max} = 1$ ,  $z_{\min} = 5.8$  cm,  $r_c = 0.45R - 0.022$ ,  $f_s = 49.4$  kHz,  $c = 343.5$  m/s. For simulations, 100-iteration Monte-Carlo simulation study is employed and the curve-fitting TOF estimate method is used. First, the linear configuration of the transducers are used to estimate the range, deviation angle, and radius of curvature by Equations 6-8 respectively. Then, the central, left, and right transducers are rotated around their centers by the angles found by Equations 7,9, and 10 respectively. Finally, the estimates for rotated configuration are calculated again by using Equations 6-8. From now on, the first estimate corresponds to the estimate taken by the linear configuration, and second estimate corresponds to the estimate taken by the rotated configuration. In all simulations, dashdot (or

dot) and dashed lines indicate the mean of the estimate and  $\pm s$  (standard deviation) for the linear and rotated positions respectively.

Figures 4(a) and (b) illustrates the radius of curvature estimates when the thresholding method is used in the absence and presence of noise respectively. The first estimate worsens after  $d = 37$  cm in the absence of noise while second estimate continues improving. The error in the first estimate is 22.8% while it is 9.2% for the second estimate. In the presence of noise, the second estimate provides approximately 40% better results. Also, the standard deviation is less for the second estimate. Figures 5(a) and (b) shows the same results when the curve-fitting method is used to estimate TOF in the absence and presence of noise respectively. In the absence of noise, the first estimate gets worse after 43cm (it was 37 for the thresholding method). The error is 11.2% for the first estimate and it is 0.4% for the second estimate. In the presence of noise, the second estimate is better than the first estimate. Comparison of Figure 4(b) and 5(b) shows that the curve-fitting method provides better estimates than that of the thresholding method. The improvements are approximately 60% and 20% for the first and second estimates respectively.

**Figure 4.**  $R$  estimate versus  $d$  with thresholding in the absence (a) and presence (b) of noise.

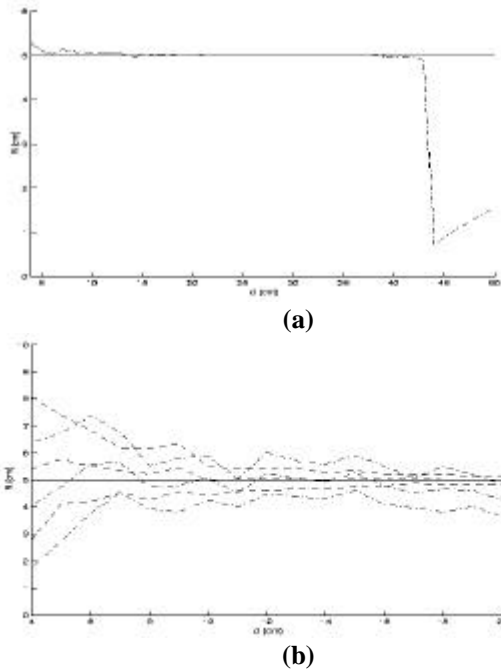


**Figure 5.**  $R$  estimate versus  $d$  with curve-fitting in the absence (a) and presence (b) of noise.

Figure 6(a) illustrates the range estimate  $r$  versus transducer separation  $d$ . The curve-fitting method is employed for TOF estimates. The first estimates improve until  $d = 12$  cm and then it worsens since now the target is located at a very low SNR region.  $R = 5$  cm,  $q = 5^\circ$  are considered. Figure 6(b) shows the range estimate  $r$  versus deviation angle  $q$ .  $R = 5$  cm and  $d = 10$  cm are considered. When  $q = 6^\circ$ , the left and when  $q = 12^\circ$ , the right transducer start measuring wrong.

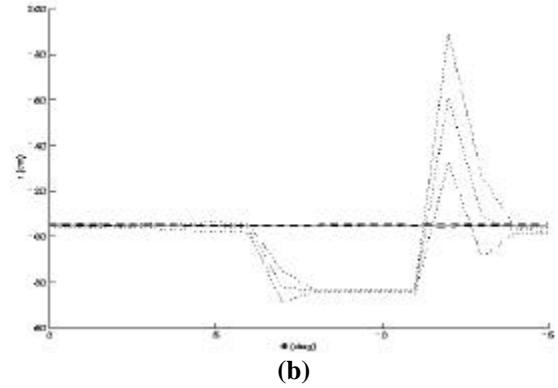
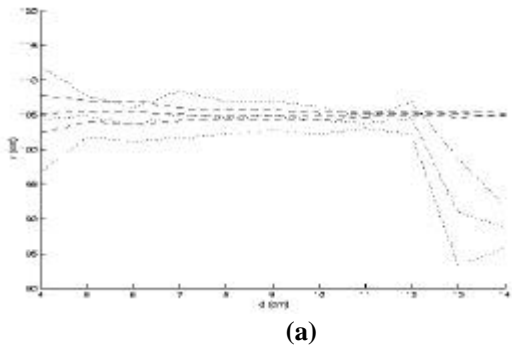


**Figure 6.**  $r$  estimate versus (a)  $d$  (b)  $q$ .

## 7. Experimental Results

### 7.1. Experimental Set-up

The set-up is constructed for 3D applications. The unit consists of five transmitter/receiver Polaroid transducers with the resonant frequency 49.4 kHz. The central transducer is flanked by four transducers symmetrically as shown Figure 7. Only the left, central, and right transducers are used for the experiments. A 4-channel DAS-50 A/D card with 12-bit resolution and 1 MHz sampling frequency is used to sample the echo signals.

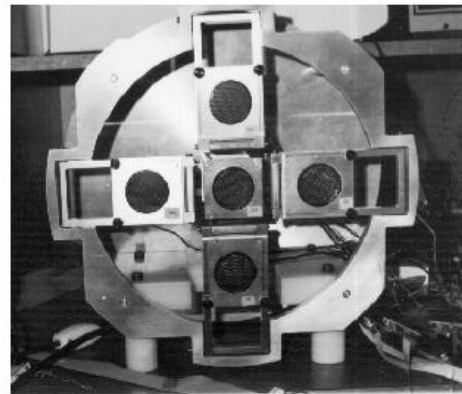


**Figure 7.** The experimental set-up.

### 7.2. Results

Table 1 displays some experimental results for the radius of curvature estimate of a cylindrical object with radius 50 mm when the transducer separation is 10 cm. The curve-fitting method is employed for TOF estimate. In the table,  $\hat{R}_1$  and  $\hat{R}_2$  correspond to the radius of

curvature estimates of the linear and rotated configurations respectively. It is concluded that the estimates are improved by the adaptive configuration.

**Table 1.** Experimental results for a cylinder of  $R = 50$  mm and  $d = 7.5$  mm.

$h_o$ (mm)	$E(\hat{R}_1)$ (mm)	$S_{\hat{R}_1}$ (mm)	$E(\hat{R}_2)$ (mm)	$S_{\hat{R}_2}$ (mm)
300	<b>48.27</b>	<b>6.84</b>	<b>48.93</b>	<b>4.10</b>
400	<b>51.13</b>	<b>10.08</b>	<b>50.27</b>	<b>6.25</b>
500	<b>49.17</b>	<b>15.23</b>	<b>49.44</b>	<b>9.29</b>
600	<b>52.33</b>	<b>22.43</b>	<b>51.79</b>	<b>13.24</b>
700	<b>44.96</b>	<b>27.61</b>	<b>46.63</b>	<b>16.57</b>
800	<b>44.55</b>	<b>35.02</b>	<b>48.36</b>	<b>21.52</b>
900	<b>50.64</b>	<b>45.42</b>	<b>50.25</b>	<b>26.80</b>
1000	<b>59.87</b>	<b>57.41</b>	<b>55.48</b>	<b>33.39</b>

## 8. Conclusion

In this study, radius of curvature and location estimates of cylindrical objects by a multi-sensor sonar system has been investigated. Two methods of TOF has been used and it has been shown that the curve-fitting method improves TOF estimate. Moreover, the adaptive configuration decreases the effect of low angular resolution of sonar sensors considerably. The results are useful for target discrimination especially for primitive types such as walls and edges. For high values of curvature, the target is assumed to be a planar wall, and for values close to zero, the target is assumed to be an edge. The method can be generalized to spherical objects as well [8].

## References

- [1] R. Kuc, "Fusing binaural sonar information for object recognition", *Proceedings of IEEE/SICE/RSJ international Conference on Multisensor Fusion and Integration for Intelligent Systems*, 1996, pp. 727-735.
- [2] L. Kleeman, and R. Kuc, "Mobile robot sonar for target localization and classification", *International Journal of Robotics Research*, August 1995, vol. 14, pp. 295-318.
- [3] A. M. Flynn, "Combining sonar and infrared sensors for mobile robot navigation", *International Journal of Robotics Research*, December 1988, vol. 7, pp. 5-14.

[4] A. M. Sabatini, "A digital signal processing technique for compensating ultrasonic sensors", *IEEE Transactions on Instrumentation and Measurement*, 1995, vol. 44, pp. 869-874.

[5] H. Peremans, K. Audenaert, and J. M. Van Campenhout, "A high resolution sensor based on tri-aural perception", *IEEE Transaction on Robotics and Automation*, February 1993, vol. 9, pp. 36-48.

[6] B. Barshan, *A Sonar-Based Robot for Bat-like Prey capture*, PhD tehsis, Yale University, New Haven, CT, December 1991, University of Michigan Microfilms, order number 9224325.

[7] B. Barshan, and R. Kuc, "A bat-like sonar system for obstacle localization", *IEEE Transactions on Systems, Man and Cybernetics*, July/August 1992, vol. 22, no. 4, pp. 636-646.

[8] B. Barshan, A. S. Sekmen, "Radius of curvature estimation and localization of targets using multiple sonar sensors", *The Journal of the Acoustical Society of America*, April 1999, vol. 105, no. 4.